Disorder and electronic properties of substituted perylene radical-cation salts

V. Ilakovac,* S. Ravy, and A. Moradpour
Laboratoire de Physique des Solides (URA CNRS 02), bât. 510, Université Paris-Sud, 91405 Orsay Cedex, France

L. Firlej and P. Bernier
Groupe de Dynamique des Phases Condensées (URA CNRS 233) USTL, Place Eugène Bataillon, 34060 Montpellier Cedex, France
(Received 5 December 1994)

We present an x-ray diffuse scattering study of the one-dimensional substituted perylene radical-cation $(M)_2X$-S salts, where M is the 1,2,7,8-tetrahydrodicyclopenta[cd,lm]-perylene or the 3,4,9,10-tetramethylperylene radical cation, X the PF_6^- or AsF_6^- anion, and S a solvent molecule similar to CH_2Cl_2. These isostructural salts consist of stacks of radical cations and of anion and/or solvent chains (X/S) located in the channels between the organic stacks. Despite the similarity of the TMP and CPP radical cations, the magnetic and electronic properties of both types of salts differ. We show that the structural difference between the TMP and the CPP salts resides in the transverse correlations between the positions of the X/S chains: the X/S chains are much more disordered in the TMP salts than in the CPP ones. We have studied the X/S chains disorder by using an Ising model on a triangular lattice with nearest and next-nearest neighbor interactions. This study shows that the disorder in the TMP salts is due to a competition between the direct interactions between the chains X/S and those which are mediated by the organic stacks. In the more ordered CPP salts, the later interactions are screened by the conducting electrons of the organic stacks. Accordingly, it is suggested that the TMP stacks undergo a site charge localization ($4k_F$-site charge localization). This interpretation is consistent with ^{13}C cross polarization magic angle spinning NMR, conductivity and electrochemical measurements. The consequences on the Peierls instabilities of both salts are briefly discussed.

I. INTRODUCTION

Metallic conductivity in low-dimensional organic compounds has been obtained in the 1970's (Ref. 1) in charge-transfer salts of the TTF-TCNQ family. In these materials, the metallic character is due both to the overlap of the π orbitals of the organic molecules in the direction of the chain (characterized by the transfer integral t) and to weak on-site electron-electron repulsion (represented by the repulsion energy U). However, the metallic state was found to be always unstable at low temperature, where insulating $2k_F$ or $4k_F$ charge-density wave (CDW) states were observed (k_F being the Fermi wave vector).[2] In radical-cation salts such as $(TMTSF)_2X$ (the so-called Bechgaard salts), where X is an inorganic anion such as PF_6^- or ClO_4^-, other electronic ground states such as superconductivity[3,4] or spin-density-wave states[5,6] have been discovered.[7] In these type of materials, comparison of isostructural salts with similar radical cations has yielded interesting information. For instance, the sulfur-based $(TMTTF)_2X$ compounds exhibit electronic localization around 200 K,[8] while the $(TMTSF)_2X$ are metallic down to about 10 K. These behaviors can be qualitatively understood as a consequence of the stronger ratio U/t of the TMTTF materials.[9] The coupling between the counter ions and the electrons of the stacks is also relevant for the understanding of the properties of the radical cation salts.[10] In the $(TMTTF)_2X$ compounds, the electronic localization is ascribed to the $4k_F$ response of the electron gas to the anionic potential.[11]

We will present here a comparative structural study of two types of isostructural salts, based on the very similar radical cations 1,2,7,8-tetrahydrodicyclopenta[cd,lm]-perylene (CPP) and 3,4,9,10-tetra-methylperylene (TMP) (Fig. 1). In a previous paper,[12] we presented a ^{13}C CPMAS NMR, (CPMAS is cross polarization magic angle spinning) study of the two salts $(CPP)_2PF_6$-CH_2Cl_2 and $(TMP)_2PF_6$-CH_2Cl_2. These two isostructural materials (monoclinic, space group $C_{2/m}$) consist of stacks of molecules (Fig. 2) in the c direction, separated by chains of alternating PF_6^- anions and CH_2Cl_2 solvent molecules

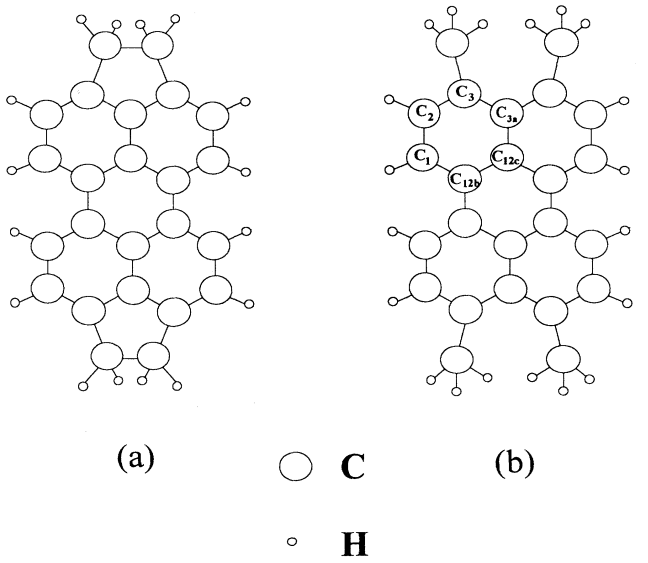

FIG. 1. CPP (a) and TMP (b) molecule.

0163-1829/95/52(6)/4108(15)/$06.00

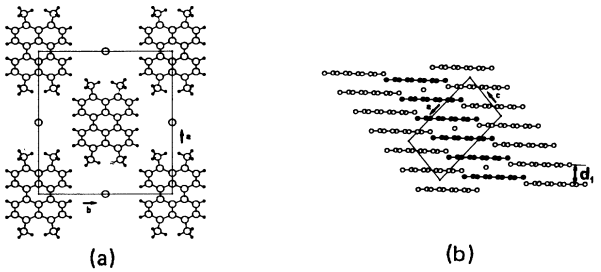

FIG. 2. Crystal structure of $(TMP)_2PF_6$-CH_2Cl_2 viewed along the c (a) axis and along the b axis (b) (from Ref. 12).

(X/S chains). In a one-electron picture, these materials have a quarter-filled band with $2\mathbf{k}_F=\mathbf{c}^*/4$ ($4\mathbf{k}_F=\mathbf{c}^*/2$). It was found that these X/S chains were more disordered in the interstack channels in the TMP salts than in the CPP one's. Moreover, solid-state ^{13}C CPMAS NMR of both salts exhibited two different locally resolved ^{13}C Knight-shifts sets.[12] In the TMP salt 14 lines were observed and in the CPP salt only seven lines were measured, as expected from the (D_{2h}) molecular symmetry. The mean values of the Knight shifts were, however, well accounted for by extended Hückel molecular-orbital calculations and were interpreted as due to the strain-induced distortions of the perylene skeleton. These results suggested that the difference in the number of ^{13}C lines might be related to the X/S disorder. In this paper, we study the correlation between the disorder of the X/S chains and the physical properties of both types of salts.

In Sec. II, we will present the experimental techniques and in Sec. III the results of the x-ray diffuse scattering study of the disorder and the influence of the nature of the anion and of the solvent on this disorder. Section IV will be devoted to the modeling of the disorder by a simple Ising model, and in Sec. V we will attempt to interpret the differences between the two type of salts.

II. EXPERIMENT

The diffuse scattering experiments were performed using the monochromatic Cu $K\alpha$ radiation ($\lambda=1.5418$ Å) obtained after a (002) reflection on a doubly bent graphite monochromator. At ambient temperature we used classical Weissenberg and precession (Buerger) methods and at low temperature (down to about 10 K) the fixed-film fixed-crystal method. Microdensitometer analysis of the x-ray photographs was performed by a transmission scanner.

Details of instrumentation for the electrochemical measurements and the crystal-growth technique were reported previously.[12] The crystals obtained have the shape of a few mm long needle (typical size is $10\times0.1\times0.1$ mm^3).

The ^{13}C NMR spectra were recorded on polycrystalline samples with a Bruker CXP spectrometer working at 50.3 MHz. High resolution in solid state was achieved using magic angle spinning (MAS, $\nu\sim2$ kHz) and cross polarization (CP) techniques (for more details see Ref. 12). The chemical shifts were referenced to tetramethylsilane (TMS).

III. RESULTS

A. PF_6^- salts

Following the previous investigation of Ref. 12, we first studied the PF_6^- derivatives of TMP and CPP. Figure 3 shows the oscillating crystal photographs for $(CPP)_2PF_6$-CH_2Cl_2 and $(TMP)_2PF_6$-CH_2Cl_2 with the **c** axis vertical. Diffuse lines with weakly modulated intensity are clearly visible at $l=n+0.5$ (n integer) between the layers of main Bragg reflections. These diffuse lines have the experimental resolution in the chain direction **c**. These features were interpreted before[12] as being due to some positional disorder of the long-range ordered X/S chains in the channels. Let us note that the absence of such diffuse lines in the Bragg layers indicates that the sites of the PF_6^- or CH_2Cl_2 species are well defined so that the anions and solvent molecules can only occupy two positions in the lattice [Fig. 2(a)]. Consequently, one has a short-range ordering (SRO) of the X/S chains in the transverse directions [i.e., in the (**a**,**b**) plane]. Although a one-dimensional long-range ordering is impossible in principle, our experimental resolution (0.01 Å^{-1}) does not enable us to estimate the true longitudinal correlation lengths of the X/S ordering in the **c** direction. In

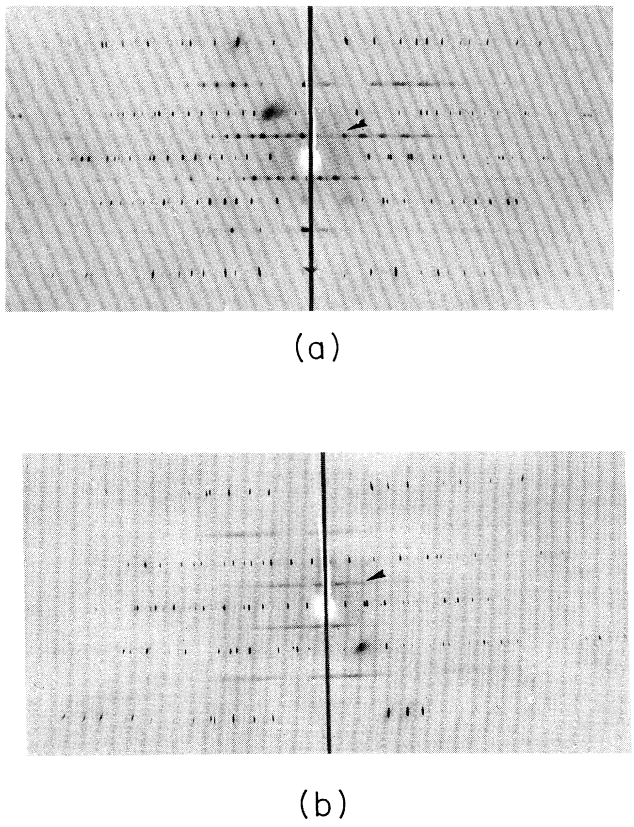

FIG. 3. Room-temperature oscillating ($\Delta\omega=40°$) crystal photographs of $(CPP)_2PF_6$-CH_2Cl_2 (a) and $(TMP)_2PF_6$-CH_2Cl_2 (b). The c axis is vertical. The arrows point towards the $l=1/2$ diffuse lines.

the following, we will consider that the X/S chains are effectively long-range ordered in the **c** direction.

More information on the SRO of the X/S chains has then been obtained from the x-ray patterns of the $l=0.5$ layers, presented in Figs. 4(a) and 5(a). Because of the two-dimensional (2D) character of the X/S disorder, we will always refer to the 2D first Brillouin zone (1st BZ) shown in Fig. 6(b), which is more adapted to our problem than the real 3D Brillouin zone.

The Weissenberg photograph for the CPP salt exhibits thin diffuse lines in the **b*** direction, resolution limited in the **a*** direction, whose maxima are located at the $h\mathbf{a}^*+k\mathbf{b}^*+0.5\mathbf{c}^*(h+k=2n+1)$ reciprocal positions, i.e., at the M point of the 1st BZ [Fig. 6(b)]. Figure 4(b) displays a microdensitometer scan in the **b*** direction around the (3,0,0.5) reciprocal position. The half width at half maximum (HWHM) of this scattering in the **b*** direction is 0.01 Å^{-1}. This profile cannot be fitted by a Lorentzian line shape [dotted line in Fig. 4(b)] that underestimates the scatterings in the wings. Instead, it can be fitted by two types of functions, either by the square

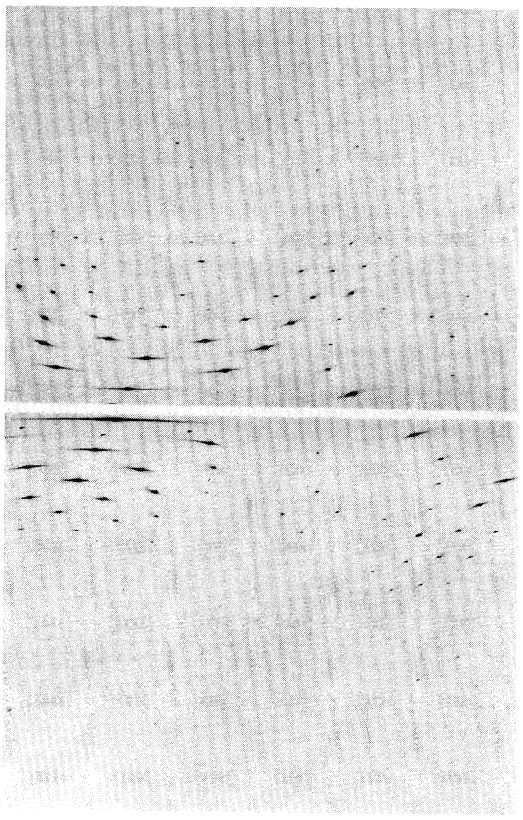

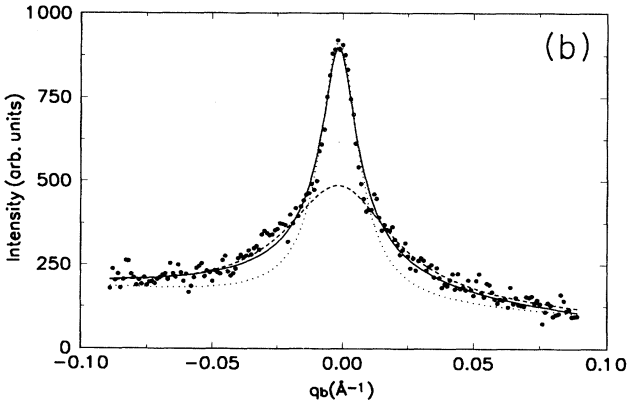

FIG. 4. (a) Weissenberg diffraction pattern of the $l=0.5$ layer of $(CPP)_2PF_6$-CH_2Cl_2. (b) Scattering intensity profile of the (3,0,0.5) reflection in the **b*** direction. The full line represents a fit by a square root of a Lorentzian function, while dotted and dashed lines represent Lorentzian functions.

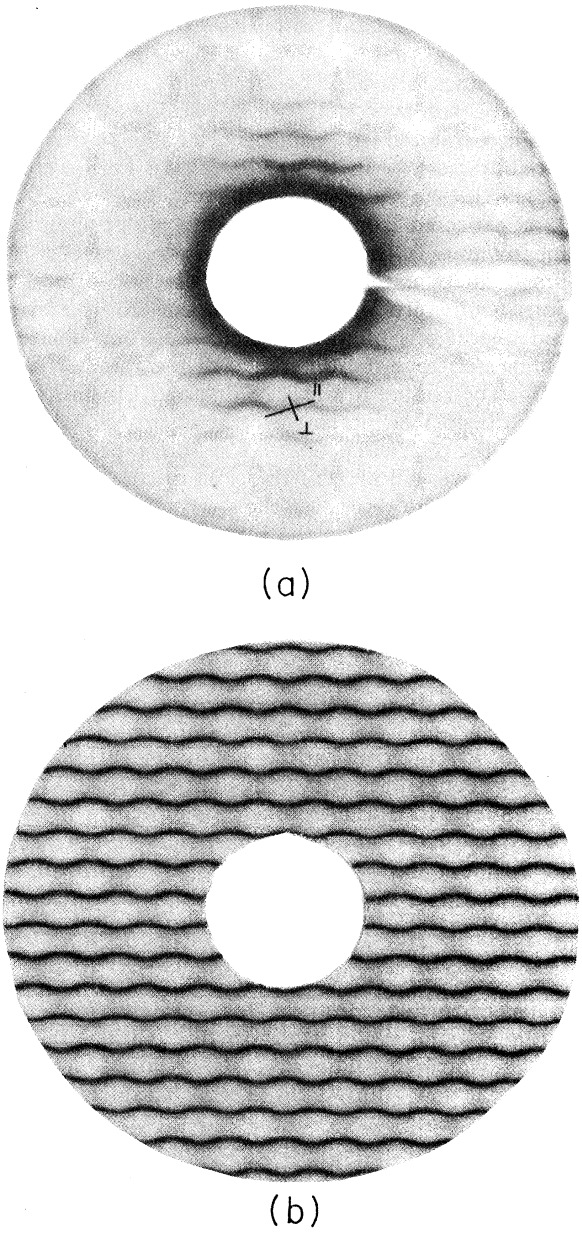

FIG. 5. Precession pattern of $(TMP)_2PF_6$-CH_2Cl_2 (a) and its best simulation (b). ⊥ and ∥ represent the directions of scans described in the text.

root of a Lorentzian (full line) or by the sum of two Lorentzians as shown in Fig. 4(b). Our experimental results do not allow us to decide which type of fit function is the best one. Nevertheless, the two types of fit imply different physical models of disorder that will be briefly discussed in Sec. IV D.

Surprisingly, the x-ray pattern for the TMP compound consists of warped lines of roughly constant intensity [see Fig. 5(a)], undulating around the $k=m/2$ lines, with small reinforcements near the C points of the 1st BZ ($\mathbf{a}^*/2\pm\mathbf{b}^*/2$ reciprocal positions). A simple analysis of this scattering clearly indicates the more disordered character of X/S chains of the TMP salt as suggested in our previous study.[12] Half width at half maximum (HWHM) have been determined by microdensitometer analysis in directions indicated in Fig. 5(a). The inverse of the HWHM's gives us an estimate of the correlation lengths in the corresponding directions. One finds $\xi_{\parallel}\cong 17$ Å and $\xi_{\perp}\cong 100$ Å.

B. Effect of the anion and solvent size

In order to understand the nature of the disorder we decided to prepare other CPP and TMP salts with anions and solvents of different sizes. The AsF_6^- and SbF_6^- anions and CH_2Cl_2, CH_2ClBr, CH_2Br_2, and $CHCl_3$ solvent molecules were used to synthesize new salts of the family. The results of this study are summarized in Tables I and II.

1. TMP salts

The precession pattern of the $l=0.5$ layer for $(TMP)_2AsF_6$-CH_2Cl_2 is shown in Fig. 7(a). Broad diffuse scattering around the M points of the 1st BZ ($h\mathbf{a}^*+k\mathbf{b}^*+0.5\mathbf{c}^*$ with $h+k=2n+1$) is clearly visible. More precisely, the diffuse scattering exhibits a slight splitting in the $\mathbf{b}^*$ direction, the maximum of intensity being at the T'^+ and T'^- points of the 1st BZ [see Fig. 6(b)], corresponding to the $\mathbf{a}^*\pm\delta\mathbf{b}^*$ reciprocal positions. Compared to the PF_6^- salt the qualitative aspect of the x-ray pattern has changed but a strong disorder is still present. We have fitted the intensity profiles in the $\mathbf{a}^*$ and $\mathbf{b}^*$ directions by the function

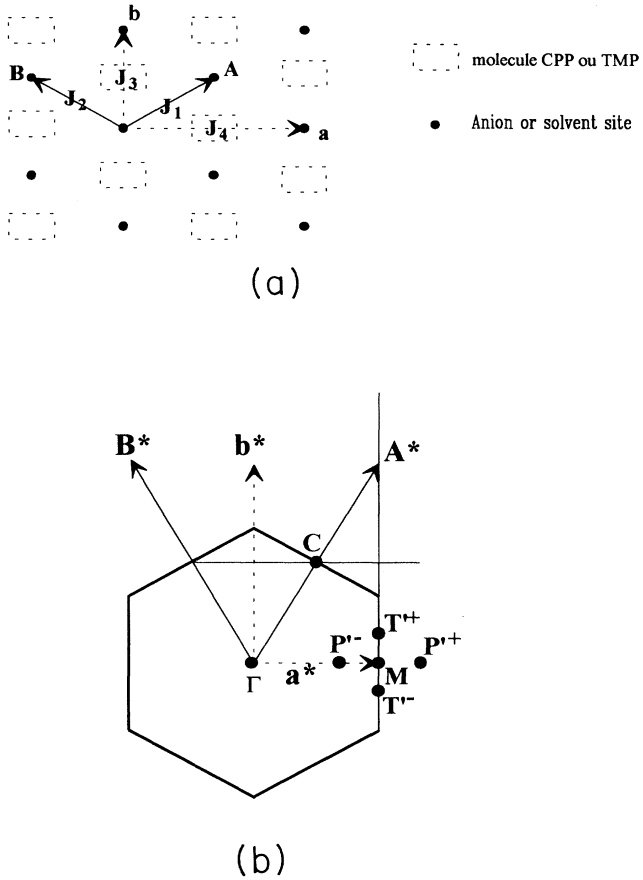

FIG. 6. (a) Primitive unit cell (**A**,**B**) with phenomenological J_i interactions. (b) sketch of the first Brillouin zone (1st BZ) of the 2D (**A**,**B**) lattice. The special points described in the text are indicated.

$$\chi(h,k)=\frac{1}{1+(h/\lambda)^2-(k/\delta_1)^2+(k/\delta_2)^4}\ , \qquad (1)$$

multiplied by a parabolic function in order to simulate in a simple way the smooth variation of the diffuse scattered intensity. The result, shown in Fig. 8, gives $\lambda=0.17$, $\delta_1=1.4$, and $\delta_2=0.4$. The reciprocal values of the

TABLE I. Stoichiometry and unit-cell parameters of the $(CPP)_2X$-S compounds.

CPP salts	CH_2Cl_2	CH_2ClBr	CH_2Br_2	$CHCl_3$
PF_6^-	Stoichiom. 2:1 $a=16.26(1)$ Å $b=12.63(1)$ Å $c=4.43(1)$ Å $\beta=100.9°$ $V=893.9$ Å^3	Stoichiom 2:1 $c=4.50(1)$ Å	Stoichiom 3:1[a] $c=4.37(1)$ Å	Stoichiom. 3:1[a] $c=4.35(1)$ Å
AsF_6^-	Stoichiom. 2:1 $a^*=0.062$ Å^{-1} $b=12.80(1)$ Å $c=4.45(1)$ Å $V=918.7$ Å^3	Stoichiom 3:1[a] $c=4.45(1)$ Å		

[a]Values from x-ray rotating crystal patterns.

TABLE II. Stoichiometry and unit-cell parameters of the $(TMP)_2X$-S compounds.

TMP salts	CH_2Cl_2
PF_6^-	Stoichiom 2:1
	$a=15.81(1)$ Å
	$b=13.68(1)$ Å
	$c=4.46(1)$ Å
	$\beta=101.3°$
	$V=893.9$ Å^3
AsF_6^-	Stoichiom 2:1
	$a^*=0.063(1)$ Å^{-1}
	$b=13.71(1)$ Å
	$c=4.49(1)$ Å
	$V=975.1$ Å^3
SbF_6	Stoichom 5:4[a]
	$c=4.33(1)$ Å

[a]Values estimated from x-ray rotating crystals patterns.

HWHM's give a rough approximation of the correlation lengths and one gets $\xi_a=14.7$ Å and $\xi_b=5.5$ Å. This type of fitting function is generally used when a system is close to a so-called Lifshitz line.[13,14] We will discuss this shape of the profile intensity in Sec. IV C.

The ^{13}C CPMAS NMR spectrum of $(TMP)_2AsF_6$-CH_2Cl_2 is shown in Fig. 9. In spite of the change of the transverse disorder of the X/S chains, the spectrum of $(TMP)_2AsF_6$-CH_2Cl_2 salt still exhibits 14 lines, like that of $(TMP)_2PF_6$-CH_2Cl_2 salt,[12] with the relative intensity and the splitting of the lines only slightly shifted.

We have then synthesized the $(TMP)_2SbF_6$-CH_2Cl_2 salt. Rotating crystal photographs have shown that the structure of this compound is different from that of the PF_6^- and AsF_6^- salts. The lattice spacing in the needle direction was found to be 4.33 Å (see Table II), a value similar to that obtained from the other salts. However, diffuse lines were observed at $\pm 4/5\mathbf{c}^*$ instead of $\pm 1/2\mathbf{c}^*$. This suggests that the organic chain structure is the same, but that the stoichiometry of the salt is changed from 2:1 to 5:4.

2. CPP salts

As indicated in Table I, increasing the size of the solvent molecule leads to the appearance of diffuse lines at $\pm\mathbf{c}^*/3$ on the rotating crystal photographs. From the Weissenberg photographs of the $l=0$ and $l=1$ Bragg layers of $(CPP)_2PF_6$-CH_2Br_2, the unit cell of this crystal is the same as that of the 2:1 CPP salts, with very similar lattice parameters. Moreover, the intensities of the corresponding Bragg spots in $(CPP)_2PF_6$-CH_2Br_2 and $(CPP)_2PF_6$-CH_2Cl_2, salts are very similar. This indicates that the molecular stacks are the same in both salts. In the $(CPP)_2PF_6$-CH_2Br_2 salt the appearance of the diffuse lines at $\pm\mathbf{c}^*/3$ show that the stoichiometry is changed from 2:1 to 3:1. The presence of the $\pm\mathbf{c}^*/3$ diffuse lines on the rotating crystal photographs of $(CPP)_2PF_6$-$CHCl_3$ and $(CPP)_2AsF_6$-CH_2ClBr suggests the same change of stoichiometry. A more thorough study of these materials is underway.

The three compounds $(CPP)_2PF_6$-CH_2Cl_2, $(CPP)_2PF_6$-CH_2ClBr, and $(CPP)_2AsF_6$-CH_2Cl_2 were found to have the same structure and the same type of diffuse scattering features. However, a decrease of the intensity of the diffuse lines was observed from the first to the third salt. $(CPP)_2AsF_6$-CH_2Cl_2 is the most ordered crystal of the family that we have synthesized.

The tables show that the loss of the 2:1 stoichiometry occurs when the spacing between the molecule in the **c** direction—imposed by the anion size—exceed 4.50 Å and gives evidence that the structure is controlled by this distance. This feature is not observed for the TMTTF/TMTSF salts, in which the structure is independent on the anion size.[15]

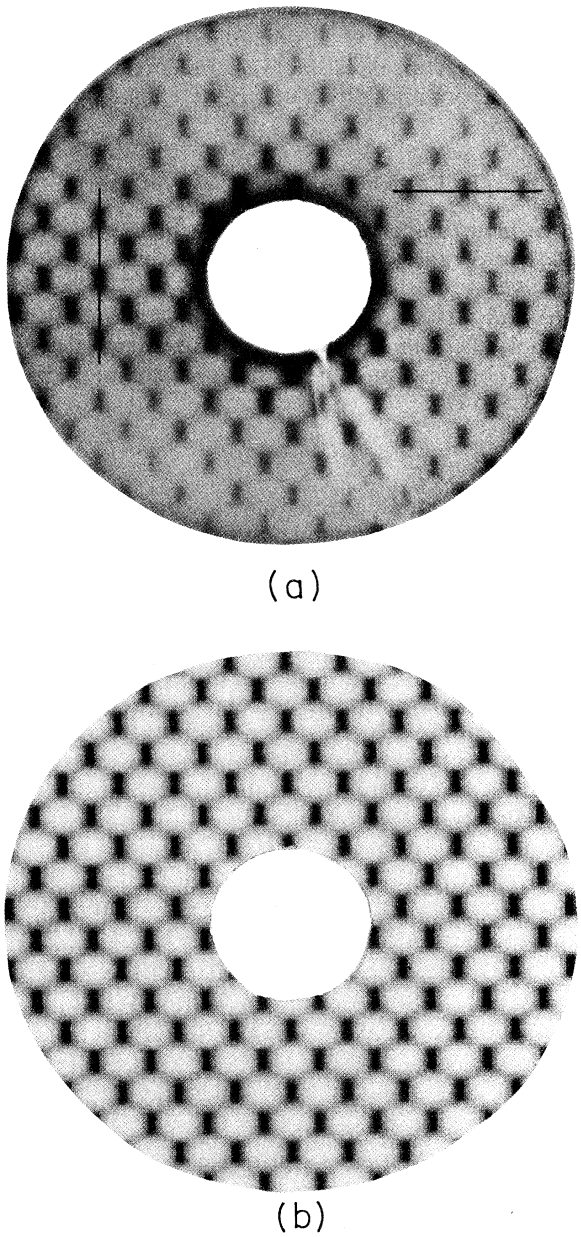

FIG. 7. Precession pattern of $(TMP)_2AsF_6^-CH_2Cl_2$ (a) and its best simulation (b). Vertical and horizontal lines represent the directions of the microdensitometer scans showed in Fig. 8.

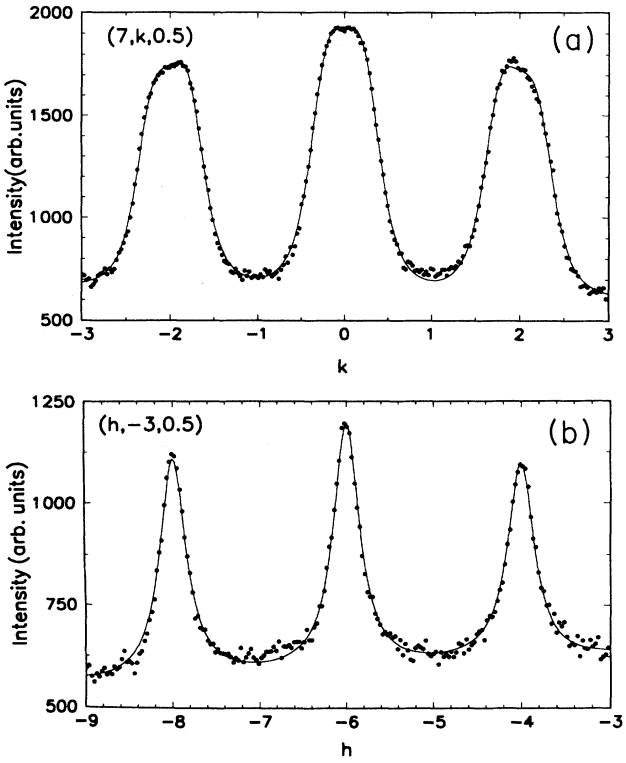

FIG. 8. Scattering intensity profile of $(TMP)_2AsF_6$-CH_2Cl_2 along: (a) the vertical line showed in Fig. 7(a), centered at the wave vector $7\mathbf{a}^*+0.5\mathbf{c}^*$, (b) the horizontal line showed in Fig. 7(a), centered at the wave vector $-3\mathbf{b}^*+0.5\mathbf{c}^*$. The solid lines are the fit by the $\chi(h,k)$ function [see Eq. (1) in the text] multiplied by a parabolic function plus a linear background.

In conclusion, this study shows that the transverse disorder of the X/S chains *depends on the radical-cation only*. By changing the anion or the solvent size, we have succeeded neither to disorder the CPP salts (the compound does not disorder but changes in structure) nor to order the TMP salts.

C. Electrochemical results

In order to understand the difference between the TMP and the CPP molecule we carried out electrochemical analysis with special attention paid to $\Delta E_{1/2}=(E_{1/2})_2-(E_{1/2})_1$, the difference between second and first oxidation potential. The results are summarized in Table III. The quantity $\Delta E_{1/2}$ gives an estimate of the intramolecular Coulomb repulsion energy U. The latter value, which is significantly higher for TMP (0.65 V) as compared to CPP (0.56 V), suggests that Coulomb repulsion is lower for CPP, that is this molecule is more polarizable than the TMP one.[16,17]

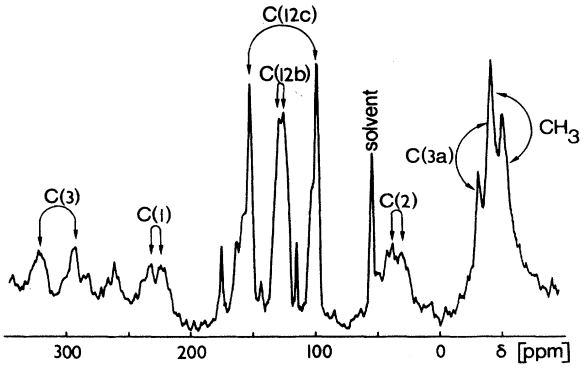

FIG. 9. ^{13}C-CPAS-NMR spectrum of $(TMP)_2AsF_6$-CH_2Cl_2. The atomic numbering scheme is given in Fig. 1(b).

D. Peierls instability

X-ray diffuse scattering patterns reveal in both CPP and TMP compounds the presence of diffuse lines at $\pm\mathbf{c}^*/4$ from the layers of Bragg reflections [Fig. 10(a)]. In CPP they condense in satellite reflections at the reduced wave vector $\mathbf{q}_P=(0,1/2,1/2)$ at 158 K for $(CPP)_2PF_6$-CH_2Cl_2 (Ref. 18) and at 170 K for $(CPP)_2AsF_6$-CH_2Cl_2 [Fig. 10(b)]. The temperature dependence of the (0,1/2,1/2) satellite reflection intensity is shown in Fig. 10(c). This quantity is proportional to the square of the order parameter of the Peierls transition. In the case of TMP salts, $2k_F$ diffuse lines appear at about 200 K but do not condense at low temperature down to 20 K.

IV. MODELING THE DISORDER

A. Motivation

The diffuse scattering measured in the $(TMP)_2PF_6$-CH_2Cl_2 and $(TMP)_2AsF_6$-CH_2Cl_2 compounds is unusual. In $(TMP)_2AsF_6$-CH_2Cl_2, the fit of the scattering in the $\mathbf{b}^*$ direction [Fig. 8(a)] by a Lorentzian function with a q^4 term [Eq. (1)] suggests the presence of competing interactions in the system.[13,19] As far as the $(TMP)_2PF_6$-CH_2Cl_2 is concerned, the unusual warped shape of the diffuse scattering cannot clearly be fitted by classical or modified Lorentzian functions. These unique types of diffuse scattering deserve more attention. In this respect, we have developed a model of disorder based on the Ising model with competing interactions that accounts for the observed diffuse scattering of the TMP salts, including the main features of the CPP salts. A mean-field analysis is first presented and, to go beyond this approximation, the results of more quantitative Monte Carlo (MC) simulations are used to obtain the parameters of the model.

TABLE III. Electrochemical results.

Compound[a]	$(E_{1/2})_1$[b,c] (V)	$(E_{1/2})_2$[b,c] (V)	$\Delta E_{1/2}$ (V)
perylene	+0.98	+1.52	0.54
CPP	+0.50	+1.06	0.56
TMP	+0.69	+1.34	0.65

[a]All compounds are approximately 1 mM in CH_2Cl_2 (in acetonitrile for perylene), with 0.1 M tetrabutylammonium hexafluorophosphate.
[b]Potentials measured vs satured calomel electrode; the present values of the first oxidation potentials are corrected, as compared to the previous overestimated values (Ref. 12).
[c]Scan rates of 100 mV s^{-1}.

B. Expression of the diffuse scattering

For the sake of simplicity, let us introduce a primitive unit cell as indicated in Fig. 6(a) with direct and reciprocal parameters defined by

$$\begin{cases} \mathbf{A}=(\mathbf{a}+\mathbf{b})/2 \\ \mathbf{B}=(\mathbf{b}-\mathbf{a})/2 \\ \mathbf{C}=2\mathbf{c} \end{cases} \text{ and } \begin{cases} \mathbf{A}^*=\mathbf{a}^*+\mathbf{b}^* \\ \mathbf{B}^*=\mathbf{b}^*-\mathbf{a}^* \\ \mathbf{C}^*=\mathbf{c}^*/2 \end{cases}, \tag{2}$$

and the origin of the lattice taken on a X/S site. In this model, we assume that the diffuse scattering in the $l=0.5$ layers is only due to the disorder of the X/S chains. It means that we neglect an eventual 2c periodicity of the molecular stacks due to dimerization or any other structural distortion with the $\mathbf{c}^*/2$ wave vector.

The shift of the disordered X/S chains in the c direction will be characterized by a pseudospin variable defined by $S_{\mathbf{r}}=1(-1)$ if a S solvent (X anion) is located at $\mathbf{r}=U\mathbf{A}+V\mathbf{B}$ (U and V integers). It is shown in Appendix A that the intensities of the Bragg spots and the diffuse scattering are given by the following formulas:

If $s_3=2n$ $I_{\text{Bragg}}=|F_X(\mathbf{s})+F_S(\mathbf{s})+2F_M(\mathbf{s})|^2$, (3a)

$$I_{\text{DiffScat}}=0 . \tag{3b}$$

If $s_3=2n+1$

$$I_{\text{Bragg}}=0 ,$$

$$I_{\text{DiffScat}}=|F_X(\mathbf{s})-F_S(\mathbf{s})|^2\sum_{\mathbf{r}}\langle S_0S_{\mathbf{r}}\rangle e^{2i\pi\mathbf{s}\cdot\mathbf{r}} , \tag{4a}$$

$$=|F_X(\mathbf{s})-F_S(\mathbf{s})|^2\langle S_{\mathbf{s}}S_{-\mathbf{s}}\rangle \tag{4b}$$

where s_3 is the $\mathbf{C}^*$ coordinate of the scattering vector $\mathbf{s}=s_1\mathbf{A}^*+s_2\mathbf{B}^*+s_3\mathbf{C}^*$, $F_X(\mathbf{s})$, $F_S(\mathbf{s})$, $F_M(\mathbf{s})$ the molecular structure factors of the anion (X), the solvent (S), and the CPP or TMP (M) molecule, respectively, and $S_{\mathbf{s}}=\sum_{\mathbf{r}}S_{\mathbf{r}}e^{2i\pi\mathbf{s}\cdot\mathbf{r}}$ is the 2D Fourier transform (FT) of $S_{\mathbf{r}}$.

From expressions (3) and (4) it is clear that the qualitative features of the observed diffuse scattering are well accounted for: the diffuse scattering is observed only on the s_3-odd layers and its intensity is weak because it is proportional to the square of the structure factor difference $|F_X(\mathbf{s})-F_S(\mathbf{s})|^2$. Its s variations give $\langle S_{\mathbf{s}}S_{-\mathbf{s}}\rangle$, the FT of the pair-correlation function of the pseudospin variables $\langle S_0S_{\mathbf{r}}\rangle$. As the X/S chains are long-range ordered in the c direction, this pair-correlation function is 2D. The purpose of our model is to calculate this correlation function.

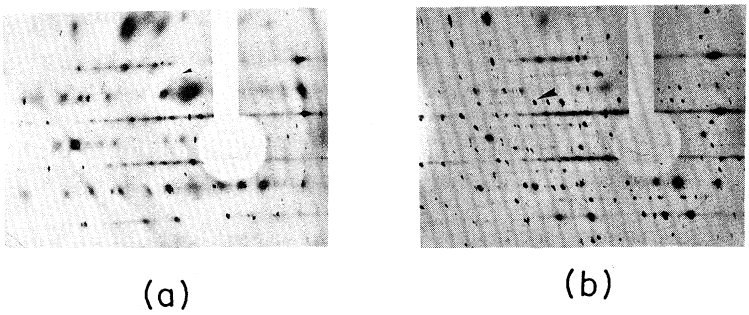

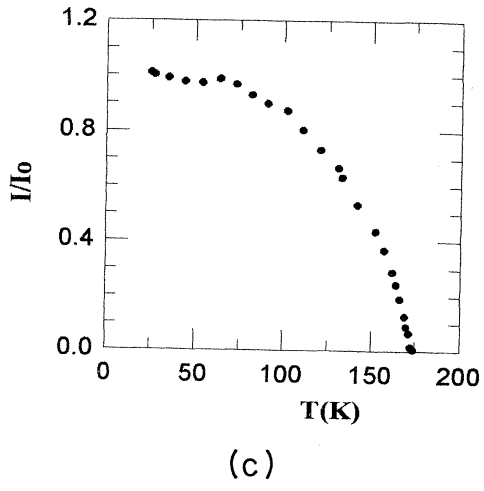

FIG. 10. Fixed-film fixed-crystal pattern of $(TMP)_2AsF_6$-CH_2Cl_2 single crystal at room temperature (a) and at 11 K (b). A small arrow points towards $2k_F$ diffuse scattering line and a large one to a low-temperature satellite reflection. Temperature variation of the normalized intensity of a satellite with temperature (c).

C. Analysis of the disorder of the TMP salts

1. Formulation of the model

Our analysis of this disorder in these materials is based on the Ising model on a triangular lattice with *competing* interactions. As previously described, the chain position can be characterized by a pseudospin variable S_r. The energy of an X/S chain is supposed to depend only on the positions—and thus on the pseudospin values—of its neighboring chains. To model this system, we have then used a phenomenological model with nearest- and next-nearest-neighbor interactions as indicated in Fig. 6(a). The energy of the system is then given by the expression

$$E=-\sum_r (J_1 S_r S_{r+\mathbf{A}}+J_2 S_r S_{r+\mathbf{B}}+J_3 S_r S_{r+\mathbf{A}+\mathbf{B}} +J_4 S_r S_{r+\mathbf{A}-\mathbf{B}}) , \quad (5)$$

$J_i (i=1,4)$ being the energy of a pair of antiparallel pseudospins in the **A**,**B**, **A**+**B** and **A**−**B** directions, respectively. We will consider only negative J_i interactions which insure their competing character. The $2/m$ symmetry of the system reduces the number of independent interactions and yields $J_1=J_2\neq J_3\neq J_4$. The nature of these interactions (direct or indirect) will be discussed in the following.

Exact solutions of the Ising model on a triangular lattice ($J_4=0$) have been obtained by Stephenson[20,21] and the temperature dependence of the correlation lengths in the **A**,**B** and **A**+**B** direction are known. Nevertheless, even in that case, no calculation of the scattering function $\langle S_s S_{-s}\rangle$ has been performed. As far as the general case, $J_4\neq 0$, is concerned, no exact solution is available. Therefore, we have reconsidered the problem by a mean-field analysis and MC simulations.[19]

The scattering function of this pseudospin assembly can be obtained from the wave-vector static susceptibility $\chi(\mathbf{s})$. Actually, from the classical limit of the fluctuation-dissipation theorem it is known that $\langle S_s S_{-s}\rangle$, which gives I_{Diffscat}, is proportional to $\chi(\mathbf{s})$. Using (4b), one has

$$I_{\text{DiffScat}}(s)=|F_X(\mathbf{s})-F_S(\mathbf{s})|^2 kT\chi(\mathbf{s}) . \quad (6)$$

A mean-field analysis of $\chi(\mathbf{s})$ can give us a first approximation of this quantity. Let us remark that in this model, we have neglected the variation of the $|F_X(\mathbf{s})-F_S(\mathbf{s})|^2$ term that we did not exactly know, but which gives only a slight modulation of the $\chi(\mathbf{s})$ function.

2. Mean-field analysis

The random-phase approximation gives the following expression for the static susceptibility of such a system of spins:

$$\chi(\mathbf{s})=\frac{\beta}{1-\beta J(\mathbf{s})} , \quad (7)$$

where

$$J(\mathbf{s})=2J_1\cos(2\pi s_1)+2J_2\cos(2\pi s_2) +2J_3\cos[2\pi(s_1+s_2)]+2J_4\cos[2\pi(s_1-s_2)] \quad (8)$$

is the Fourier transform of the interaction energies. In this approximation, expected to be correct at high temperature, the positions of the maxima of the diffuse scattering are given by the s coordinates which maximize the $J(s_1,s_2)$ function. Therefore, these positions are independent on temperature. We have calculated the position of these maxima in the 1st BZ as a function of the reduced constants $J_3/|J_1|$ and $J_4/|J_1|$. The results are summarized on the phase diagram displayed in Fig. 11(a), restricted to the negative values of J_i. The diagram exhibits four different domains.

In the M domain, defined by $J_3/|J_1|\geq -1/2$ and $J_4/|J_1|\geq -1/2$, the maximum of intensity is at the M point of the 1st BZ. The local ordering of the pseudospins corresponds to fluctuations around an "antiferromagneticlike" order [Fig. 12(a)], as expected if the negative $J_1=J_2$ interactions are dominant.

In the T' (resp P') domain, the scattering splits in the **b*** (resp **a***) direction and the maxima are at the T'^- and T'^+ points of the 1st BZ (resp P'^- and P'^+ points), corresponding to the $\mathbf{a}^*\pm(1/\pi)\cos^{-1}(J_1/2J_3)\mathbf{b}^*$ [resp $\mathbf{a}^*\pm(1/\pi)\cos^{-1}(J_1/2J_4)\mathbf{b}^*$] reciprocal positions [Fig. 6(b)]. The $J_3/|J_1|=-1/2$ and the $J_4/|J_1|=-1/2$ lines are Lifshitz lines ($\mathcal{L}$), defined as the locus of the phase digram where a splitting of the scattering appears.[19,22] Let us remark that x-ray diffuse scattering of $(TMP)_2AsF_6$-CH_2Cl_2 corresponds qualitatively to the scattering by a system of pseudospins with interaction energies in the T' domain.

The T' and P' domains are separated from the C domain, where the scattering is maximum at the C point of the 1st BZ by the line ($\mathcal{D}_2$) of equation $4J_3J_4-J_1^2=0$.

The line $\mathcal{D}_2$ is the boundary between two domains in which the pseudospin fluctuations are *qualitatively* different. We will call such a line a *disorder line of the second kind* by analogy to the definition of Stephenson.[21] The shape of the scattering on the disorder line can been obtained by rewriting $J(s_1,s_2)$ as

$$J(\mathbf{s})=4J_3\{\cos[\pi(s_1+s_2)]+\frac{J_1}{2J_3}\cos[2\pi(s_1-s_2)]\}^2 + \left[4J_4-\frac{J_1^2}{J_3}\right]\cos[2\pi(s_1-s_2)]^2-2J_3-2J_4 , \quad (9)$$

which gives

$$J(\mathbf{s})=4J_3\left[\cos[\pi(s_1+s_2)] +\frac{J_1}{2J_3}\cos[2\pi(s_1-s_2)]\right]^2-2J_3-2J_4 , \quad (10)$$

on the disorder line. From this expression, it is clear that the maxima of scattering are located on curves of the equation

$$\cos[\pi(s_1+s_2)]+\frac{J_1}{2J_3}\cos[2\pi(s_1-s_2)]=0\ . \qquad (11)$$

which are warped lines, running along the **b*** direction if $J_3/|J_1|>-1/2$ [Fig. 11(f)] and along the **a*** one if $J_3/|J_1|<-1/2$ [Fig. 11(d)]. The lines of maximum scattering in Fig. 11(d) have exactly the same shape as those observed in the x-ray pattern of $(TMP)_2PF_6$-CH_2Cl_2.

From this mean-field analysis, the qualitative features of the x-ray pattern of the TMP salts are accounted for, which supports the relevance of the Ising model in our problem. Nevertheless, as it is shown in Appendix B, the mean-field approximation predicts wrong ground states for the 2D Ising model, temperature-independent Lifshitz and disorder lines,[19] [let us remark that, rigorously, the disorder and Lifshitz temperatures (T_D^1,T_D^2,T_L) for different J_i interactions define disorder and Lifshitz surfaces in the $(J_3/|J_1|,J_4/|J_1|,T/|J_1|)$ diagram] and thus the wrong estimation of the J_i interactions for given diffuse scattering patterns. Therefore, we carried out computer simulations in order to get more quantitative values of the J_i interactions for a system at ambient temperature.

3. *Monte Carlo simulations*

The Monte Carlo (MC) simulations have been performed following the usual Metropolis procedure[23] in order to obtain at any temperature T the distribution of the X/S chains in a (**A**,**B**) plane. However, as we were dealing with very disordered systems we started from a large randomly disordered lattice [1024*1024(**a**,**b**), i.e., 2 097 152 spins] that we thermalized with a rather low number of spin updatings [256 Monte Carlo steps by spin (MCS/spin)]. A fast Fourier transform (FFT) of the thermalized lattice was achieved and the result was squared to obtain S_sS_{-s}, the diffuse scattering intensity in one Brillouin zone of 2 097 152 points. At last, the statistical average $\langle S_sS_{-s}\rangle$ of the intensity was obtained by averaging this intensity on (4*4) neighboring pixels, which reduced the number of points of the Brillouin zone to 131 072. It is worth pointing out that this last step is equivalent to averaging the FT of the 16 independent 131 072 spin subsystems of the initial lattice. A similar

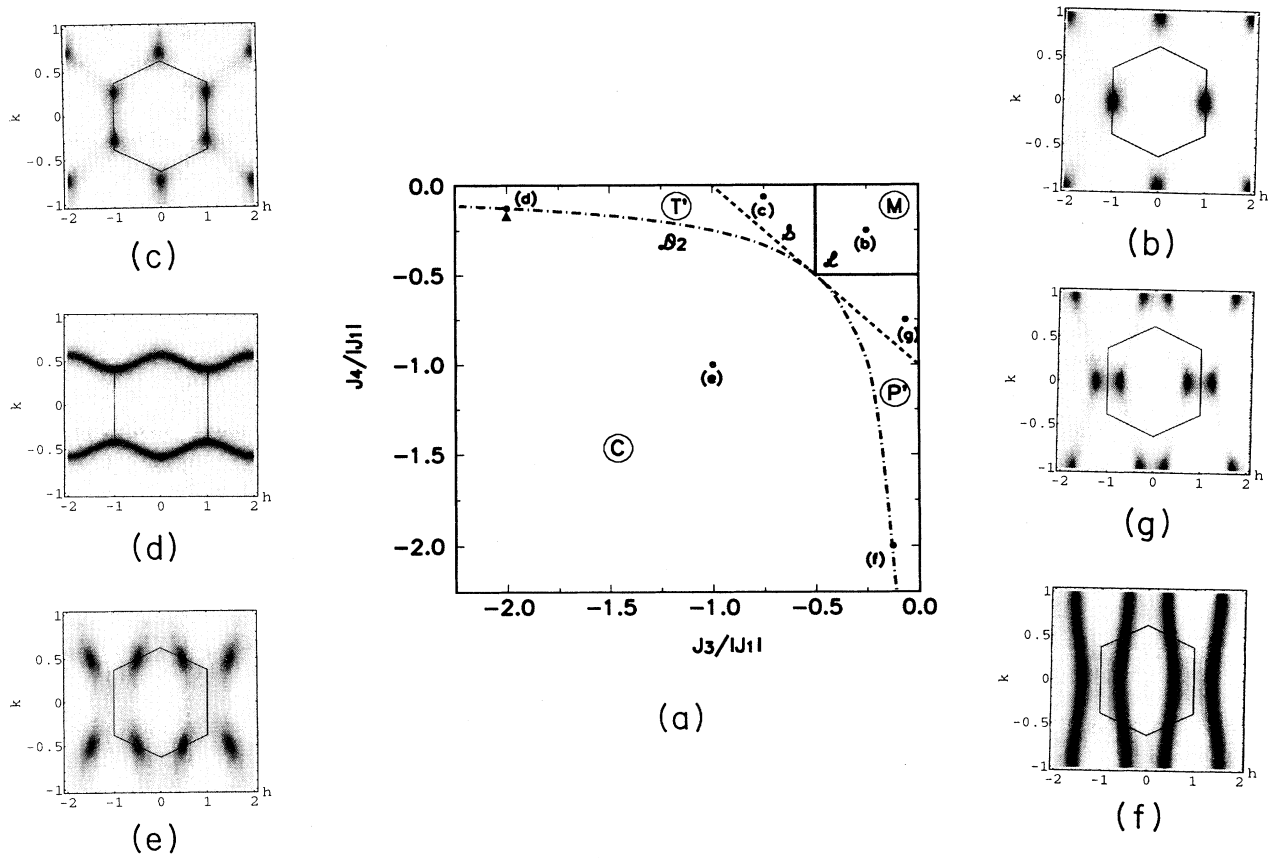

FIG. 11. (a) Mean-field $(J_3/|J_1|,J_4/|J_1|)$ phase diagram. The full lines ($\mathcal{L}$) are the Lifshitz lines, the dashed-dotted line ($\mathcal{D}_2$) is the disorder line of the second kind and the dashed ($\mathcal{S}$) line separates and M and C ground-state stability domains. The circled letters indicate the locus of the scattered intensity maxima in the 1st BZ of Fig. 6(b). The triangle indicates the position of the $(TMP)_2PF_6$-CH_2Cl_2 system in this (temperature-independent) diagram. (b), (c), (d), (e), (f), (g): Typical scattered intensity calculated at the points indicated in (a). A scheme of the 1st BZ is indicated on each figure.

procedure has been used by Butler and Welberry[24] to obtain the FT of disordered lattices. The validity of this method has been demonstrated[19] by fitting the computed intensity with the exact expression in the case $J_1=J_2, J_4=0$ at the disorder temperature of the first kind.[25]

We did not attempt to calculate precisely the temperature dependences of the disorder, Lifshitz, and transition lines for $J_4\neq 0$ by this method. Moreover, we limited ourselves to the $J_4/|J_1|\approx 0$ domain, because, as revealed by the mean-field analysis, the real systems exhibit diffuse scattering patterns corresponding to this part of the diagram. Anyway, due to the symmetry of the lattice ($J_1=J_2$) the upper condition is not restrictive: permutation of J_3 and J_4 results only in an $\mathbf{a}^*,\mathbf{b}^*$ permutation on the diffuse scattering patterns.

Let us first consider the case $J_4=0$. It is known from the exact solution that for $-1<J_3/|J_1|<0$, the ground state is an antiferromagneticlike one [see Fig. 12(a)]. Bragg reflections appear at the M point of the 1st BZ.

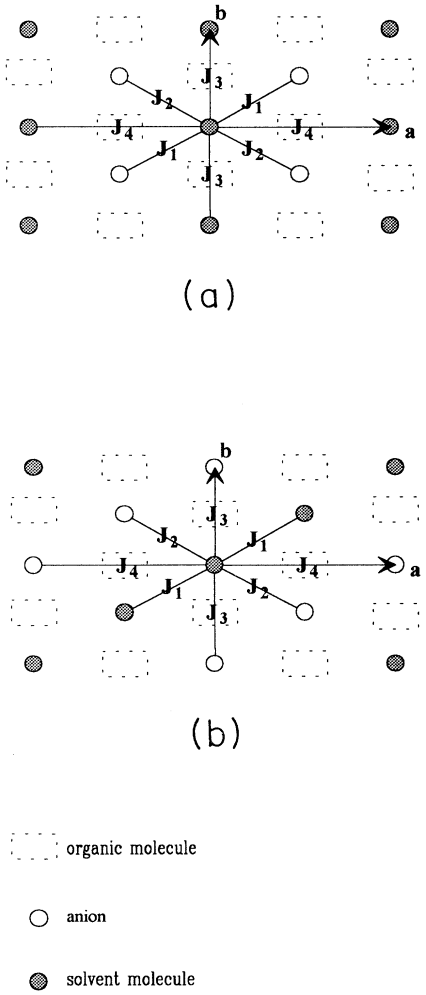

FIG. 12. Anion/solvent order in the M (a) and C (b) ground states of the system (Note that in the C region of the phase diagram *two* symmetry-related ordered domains are possible).

Above T_D^1, the *disorder point of the first kind,*[20] the pair-correlation function becomes oscillatory and behaves as

$$\langle S_0 S_{\mathbf{R}}\rangle \sim \exp[-|\mathbf{r}|/\xi_i(\mathbf{r},T)]\cos[\mathbf{q}(T)\cdot\mathbf{r}+\phi(T)]\ , \qquad (12)$$

in the **A**,**B** and **A**+**B** directions, where $\xi_i(\mathbf{r},T)$ is a correlation length and $\mathbf{q}(T)$ is a wave vector, vanishing at T_D^1. An exact expression of the diffuse scattering that we used to verify our MC procedure, is available at T_D^1.[25] This oscillatory behavior of $\langle S_0 S_{\mathbf{r}}\rangle$ is, however, difficult to evidence by scattering experiments[19] except above the Lifschitz line, where the scattering *splits* in the $\mathbf{b}^*$ direction (the maxima are located at $T'^{\pm}$ points of the 1st BZ, at the wave vector $\mathbf{q}_{As}=\mathbf{a}^*\pm\delta\mathbf{b}^*$). At variance with the mean-field analysis, the position of the Lifshitz line depends on temperature. Our MC study has located this line and shown that it only exists in the range $-1<J_3/|J_1|<-0.5$ (Ref. 19) as shown in Fig. 13.

In the case $J_4\neq 0$, the MC simulations confirm the failure of the mean-field approximation and show the temperature dependence of the disorder line of second kind. Quantitatively, in the $(J_3/|J_1|, J_4/|J_1|, T/|J_1|)$ diagram the disorder surface of second kind intercept the $T=0$ plane at the $\mathcal{S}, (J_3/|J_1|<-1, J_4=0)$ and $(J_4/|J_1|<-1, J_3=0)$ lines and approaches asymptotically the $\mathcal{D}_2$ line as the temperature goes to infinity.

Case of $(TMP)_2AsF_6$-CH_2Cl_2. The best x-ray pattern simulation [Fig. 7(b)] was obtained for the values $T/|J_1|=2.3$ and $J_3/|J_1|=-0.575$, which correspond to a point slightly above the Lifschitz line (see Fig. 13). As we did not find an analytic expression of the FT of $\chi(h,k)$, which would give us the correlation lengths in any direction, we used 1D FT of $\chi(h,0)$ and $\chi(0,k)$ to get approximate values in the $\mathbf{a}^*$ and $\mathbf{b}^*$ directions. The last FT gives us a correlation function

$$\langle S_0 S_{v\mathbf{b}}\rangle \sim \exp(-vb/\xi_b)\cos(v\mathbf{q}_0\cdot\mathbf{b}+\Phi)\ , \qquad (13)$$

with

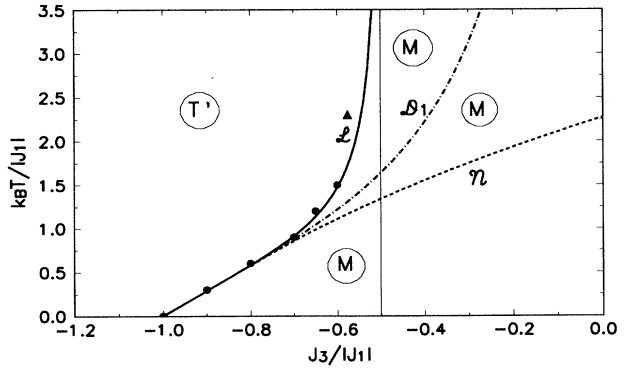

FIG. 13. $(J_3/|J_1|, T/|J_1|)$ phase diagram. Below the dashed line ($\mathcal{N}$) the antiferromagnetic ordering appears. The full line ($\mathcal{L}$) is the Lifshitz line coming from MC simulations and the dashed dotted line ($\mathcal{D}_1$) the line of disorder of the first kind. The circled letters indicate the points of maximal intensity. The triangle indicates the position of the $(TMP)_2AsF_6$-CH_2Cl_2 system in the diagram.

$$\xi_b=\frac{\delta_1}{\pi\delta_2\sqrt{2\delta_1^2+\delta_2^2}}b\ ,\quad q_0=\frac{\delta_2\sqrt{2\delta_1^2-\delta_2^2}}{2\delta_1}b^*$$

and (14)

$$\cos\Phi=\frac{\sqrt{2\delta_1^2-\delta_2^2}}{2\delta_1}(\Phi>0)\ .$$

Replacing the fitted δ_1 and δ_2 values in these relationships yields

$$\xi_a=14.7\ \text{Å}\ ,$$
$$\xi_b=7.56\ \text{Å}\ , \quad (15)$$
$$\mathbf{q}_0=0.55\mathbf{b}^*\ .$$

Comparison of these values with the unit-cell parameters $a\sim15$ Å, $b\sim13$ Å (Table II) shows that the SRO does not extend over one unit cell. The existence of the splitting of the diffuse scattering in the $\mathbf{b}^*$ direction is a direct consequence of the competition between interactions J_3 and J_1.

Case of $(TMP)_2PF_6$-CH_2Cl_2. The best simulation of the x-ray diagram has been obtained for the values $T/|J_1|=2.5$, $J_3/|J_1|=-2$, and $J_4/|J_1|=-0.17$ [Fig. 5(b)]. On the mean-field phase diagram [Fig. 11(a)], this point is located slightly below the $\mathcal{D}_2$ line.

The major conclusions of this part is that the disorder of the X/S chains either in $(TMP)_2AsF_6$-CH_2Cl_2 or in $(TMP)_2PF_6$-CH_2Cl_2 can be understood as a consequence of competing interactions between chains in the transverse **a**, **b**, and **a**±**b** directions. These competing interactions are responsible for the presence of disorder lines in a generalized $(J_3/|J_1|,J_4/|J_1|,T/|J_1|)$ phase diagram. A disorder line separates the disordered phase in two domains in which the fluctuations differ. For disorder lines of the first kind, the high-temperature short-range order has an oscillatory behavior and a nonoscillatory one below T_D^1. The later behavior becomes apparent only above the so-called Lifshitz line where the diffuse scattering splits. It is the case of $(TMP)_2AsF_6$-CH_2Cl_2. For disorder lines of the second kind, the short-range order suddenly changes at T_D^2, the disorder temperature of the second kind, so that the maximum of the diffuse scattering switches from a wave vector to another. At T_D^2, the diffuse scattering is intermediate between that of both types of order. In our study, warped diffuse lines are observed in $(TMP)_2PF_6$-CH_2Cl_2.

D. Disorder in the CPP salts

Let us analyze the diffuse scattering observed on the x-ray patterns of the CPP salts. This diffuse scattering consists of small and thin diffuse lines in the $\mathbf{b}^*$ direction, centered at the M points of the 1st BZ. These lines have the width of the Bragg reflections in the $\mathbf{a}^*$ and $\mathbf{c}^*$ directions, indicating long-range order of the X/S chains in the (**a**,**c**) planes (at the scale of our resolution of 0.01 Å^{-1}). The average structure of the salts is shown in Fig. 12(a): X/S chain positions alternate in the **A** and **B** directions.

The residual disorder in the **b** direction is difficult to interpret. As emphasized previously, two types of functions can be used to fit the profile along the $\mathbf{b}^*$ direction. The fit by a sum of two Lorentzian line shapes with two different correlation lengths indicates inhomogeneity of the X/S chain order in the crystal. On the other hand, the square root of a Lorentzian function does not correspond to any classical diffuse scattering model. However, this line shape could be an experimental artifact for it is known[26] that a bad experimental resolution in one or two directions can deform intrinsic line shapes. In our case, it is not ruled out that the intrinsic line shape of the scattering in the **b** direction is Lorentzian. This would indicate the presence of stacking faults of X/S(**a**,**c**) planes in the **b** direction. The reasons of such a disorder are yet not clear.

Whatever the exact description of the disorder, the X/S chains of the CPP salts are found to be long-range ordered in the (**a**,**c**) planes and weakly uncorrelated in the **b** direction with correlation lengths greater than 100 Å. In the framework previously described, this structure is obtained when the J_1 interactions are dominant in the system. The competing interactions are not relevant in that case.

V. DISCUSSION

In this structural study, we have shown that the transverse disorder of the X/S chains in the $(M)_2X$-S compounds mainly depends on the radical cation M. In the TMP salts, the X/S chains are very disordered with correlation lengths of a few unit cells. The disorder is slightly dependent on the anions and it is well accounted for by assuming competing interactions between X/S chains. Substituting AsF_6^- to PF_6^- changes the ratio of the interactions but not their competing character. On the other hand, the CPP salts are more ordered: the X/S chains alternate in the **A** and **B** directions and some residual disorder is present in the **b** direction. This can be interpreted by the presence of strong interactions in the **A** and **B** symmetry-related directions.

The number of ^{13}C NMR lines is also closely related to the nature of the radical cation: seven lines are found in the CPP compounds and two times more in the TMP ones. As the symmetry of the TMP and CPP molecules is D_{2h}, seven inequivalent carbons per molecule are expected. This is confirmed by ^{13}C CPMAS NMR on the unoxidized donors.[12] In the materials, the symmetry of a stack is also D_{2h}. However, in the CPP salts, the ordering of the X/S chains leads to the loss of the symmetry center of the molecules. This symmetry breaking, only due to the X/S chains positions around a stack, should give rise to 14 ^{13}C NMR lines in the CPP salts, which is not observed. On the other hand, the strong disorder of the X/S chains should lead to a large number of inequivalent carbon environments and to a broadening of the ^{13}C NMR lines. This is also not observed in the TMP salts: the ^{13}C lines are split but not broadened. These two remarks strongly suggest that the environment of a stack plays a minor role on the electron-spin distributions inside a molecule, probed by NMR. The number of ^{13}C

NMR lines and their positions are an *intrinsic* property of the radical cation *in the stack.*

Let us first discuss the nature of the phenomenological interactions J_i and the reasons for their difference in the TMP and CPP salts. First of all, the X/S chains are charged and they can interact by Coulomb interactions. In this respect, one can distinguish between the J_1 interactions, which are mainly direct and the J_3 and J_4 interactions which act *via* the radical-cation chains [see Fig. 6(a)]. Let us first consider the "direct part" of these interactions. From the knowledge of the distance between the chains and of their angle it is easy to calculate the distance between the anions in the two configurations. We find that the "direct part" of the J_1 and J_3 interactions are negative and that of J_4 is positive for both TMP and CPP salts. The J_1 interactions are believed to be the largest because the chains are closer in the **A** and **B** directions than in the **a** or **b** ones. It is clear that these distance calculations do not allow to differentiate between the two type of salts, which have very close lattice parameters. The J_3 and J_4 interactions are strongly dependent on the nature of the radical cation.

Some differences appear in considering the following characteristics: the calculated transfer integrals t between the molecular orbitals in the chains direction are larger in the CPP salts than in the TMP ones[27,28] ($t_{TMP}=0.196$ eV, $t_{CPP}=0.482$ eV). Moreover, the electrochemical results show that $\Delta E_{1/2}$ increases from 0.56 eV for CPP to 0.65 eV for TMP, which indicates that the intramolecular Coulomb repulsions U are slightly larger in the TMP species. These two conjugated results indicate a greater trend towards electronic Mott-Hubbard localization (greater U/t ratio) in the TMP salts than in the CPP ones. In this respect, it is noteworthy that the difference of the $\Delta E_{1/2}$ between TMP and CPP is the same as that between TMTTF and TMTSF.[16] This analysis is consistent with conductivity measurements.[28,29] At room temperature the values of the conductivity are $\sigma=50\ \Omega\,\mathrm{cm}^{-1}$ and $5\ \Omega\,\mathrm{cm}^{-1}$ for the $(CPP)_2PF_6$-CH_2Cl_2 and $(TMP)_2PF_6$-CH_2Cl_2 salts, respectively. The more delocalized character of the electrons of the stacks in the CPP salts suggests an effective screening of the indirect interactions J_3 and J_4. In that case the J_1 interaction dominates in the CPP salts, in agreement with the disorder study.

Let us remark that in one-dimensional metals, localizing electrons is equivalent to stabilizing a $4k_F$ CDW. In the TMTTF salts, the charge localization occurring at about 200 K (Ref. 8) is believed to correspond to a $4k_F$ *-bond* CDW [the charges are localized *between* the molecules with the $(4k_F)^{-1}$ periodicity] This $4k_F$-bond CDW is associated, via the electron-phonon coupling, to a dimerization of the TMTTF molecules in a stack, which *conserves* the inversion center between adjacent molecules, as shown in Fig. 14(a). In the TMP salts, such as a $4k_F$-bond CDW would not lead to the splitting of the NMR lines that is observed in our experiments.

Another possibility to explain the NMR splitting would be the existence of a superstructure like that observed in $(fluoranthenyl)_2PF_6$ (Ref. 30) or in $(perylene)_2PF_6$-THF.[31] In $(fluoranthenyl)_2PF_6$, this superstructure leads to a splitting of the NMR ^{13}C lines.[32] Such a superstructure has not been observed in our TMP salts, so far.

In agreement with the NMR and the diffuse scattering results, we suggest the existence of a $4k_F$ *-site* CDW [i.e., the charges are localized *on* the molecules with the $(4k_F)^{-1}$ periodicity] in the TMP salts. Unlike a $4k_F$ bond, a $4k_F$-site CDW breaks the center of symmetry between two adjacent molecules [Fig. 14(b)], which leads to a doubling of the number of inequivalent ^{13}C sites. This in turn could split the NMR lines as observed in the TMP salts.

Furthermore, due to the $(4k_F)^{-1}$ periodicity of the X/S chains, direct Coulomb interactions between the electrons of the molecular stacks and the X/S chains arise. This gives indirect mediated interactions between X/S chains in the **a** and **b** directions, contributing to the J_3 and J_4 interaction energies. The exact values of the J_3 and J_4 interactions, due to both indirect and direct cou-

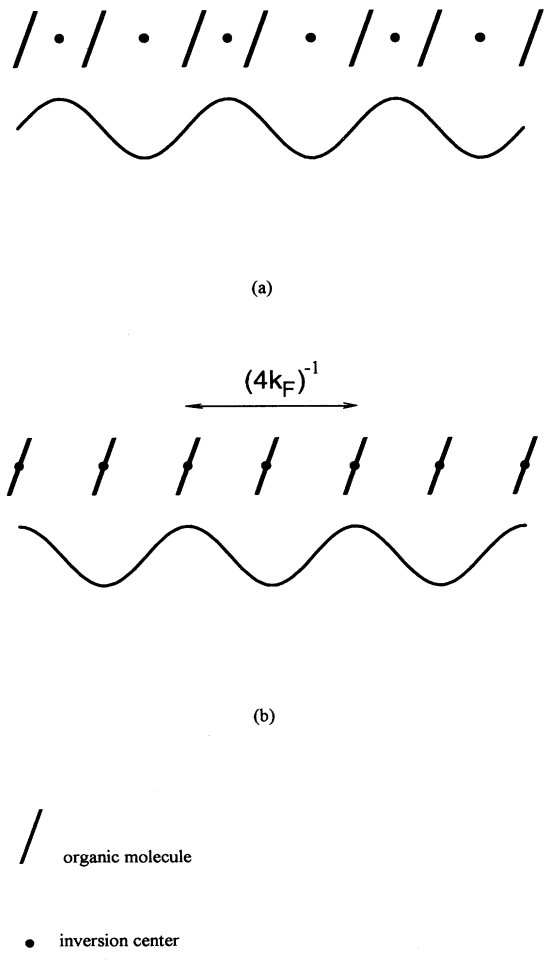

FIG. 14. Schematic representations of a $4k_F$-bond CDW (a) and a $4k_F$-site CDW (b). The charge-density modulation is represented by a sinusoid. Note that the two CDW are in quadrature.

plings, are thus strongly dependent on the exact repartition of the electronic charge on the TMP molecules. The knowledge of this repartition, which should enable us to estimate the J_i interactions is however impossible to obtain from our data. Therefore, the strong difference between the J_3 interactions in the AsF_6^- and the PF_6^- TMP salts $[J_3(PF_6^-) \propto 3J_3(AsF_6^-)]$ is difficult to explain, but could be due to a variation of the amplitude of the $4k_F$-site CDW, as the NMR results suggest. Although we lack an exact calculation of the J_i interactions, their competing character is likely due to a decrease of the screening of the indirect interactions.

Let us remark that, in principle, $4k_F$-bond or -site CDW's coupled to intra- or intermolecular distortions (as a dimerization) should contribute to diffuse scattering. However, this contribution could not be distinguished from the scattering due to the X/S chains disorder. This is the reason we neglected it in our model.

At last, let us come back to the Peierls instability in these salts. It is known that arene salts are very one-dimensional materials.[32] For example, $(fluoranthenyl)_2PF_6$ salts have a conductivity anisotropy $\sigma_\parallel/\sigma_\perp \approx 1000$,[33] and undergo a Peierls transition at 180 K, observed both by NMR (Ref. 32) and x-ray-scattering measurements.[30] In the present study, the x-ray results show that the 3D coupling of $2k_F$ CDW's occurs at about 160 K in the CPP salts and is suppressed in the TMP salts. The reason of this difference is twofold. At first, the $2k_F$ response function is reduced in the presence of a $4k_F$-site CDW as recently pointed out[34] for $[(TMTSF)_{1-x}(TMTTF)_x]_2X$ solid solutions. This effect could be responsible for the weakening of the $2k_F$ diffuse line intensity of the TMP salts. Secondly, the transverse ordering of the $2k_F$ CDW's is prevented by the transverse disorder of the X/S chains suppressing the Peierls transition.

VI. CONCLUSION

We have studied the disorder of the anion-solvent chains in the $(TMP)_2X$-S and $(CPP)_2X$-S radical cation salts with $X=PF_6^-$, AsF_6^-, SbF_6^-, and $S=CH_2Cl_2$, CH_2ClBr, CH_2Br_2, and $CHCl_3$. The purpose of this study was twofold: to understand the unusual diffuse scattering patterns observed in the TMP salts (i.e, to obtain a worthwhile description of the disorder) and to explain the difference between the NMR and diffuse scattering measurements of the CPP and the TMP salts.

We have shown by mean-field analysis and Monte Carlo simulations that modeling the interactions between X/S chains by phenomenological Ising energies J_i, allows us to obtain good fits of the ambient temperature x-ray diffuse scattering patterns of $(TMP)_2PF_6$-CH_2Cl_2 and $(TMP)_2AsF_6$-CH_2Cl_2. The direct interactions between chains (J_1) are found to dominate in the CPP salts, while competing interactions *via* the organic stacks are necessary to understand the diffuse scattering of the TMP salts. We show in particular that such diffuse scattering patterns are a direct signature of competing interactions in a system. Moreover, the concept of disorder lines, rarely used for the study of disorder, turns out to be very helpful in the interpretation of such anomalous scattering. In this respect, let us mention that changing some parameters of our model allows to account for "hexagonal" diffuse scattering observed in some layered materials.[35–37]

Considering all the physical properties of these salts, we suggest the following interpretation of our results. In the CPP salts, which have a more metallic character than the TMP salts, the interactions *via* the molecules are screened. The direct interactions between X/S chains dominate and the chains are well ordered. In the TMP salts, we propose that a *$4k_F$-site CDW* is stabilized, which gives rise to competing interactions between X/S chains in the **a** and **b** directions. This interpretation is consistent with the other physical properties of the salts and especially accounts for the ^{13}C NMR data. The Peierls transition, occurring at abut 160 K in the CPP salts, is suppressed in the TMP salts by this $4k_F$-site CDW and the transverse disorder of the X/S chains.

ACKNOWLEDGMENTS

We thank E. Canadell, C. Coulon, B. Levy, R. Moret, P. Michel, and J.-P. Pouget for useful discussions. We are indebted to T. Garel for pointing out the relevance of the mean-field analysis in our study.

APPENDIX A: FORMULATION OF THE DIFFUSE SCATTERING INTENSITY

As the X/S chains are disordered, and as the two shifts of the chain are symmetrically equivalent, the probability of occupation of the anion-solvent site by an anion is the same as that of a solvent molecule. This yields $\langle S_r \rangle = 0$.

The structure factor of an anion X, solvent S or radical cation M (CPP,TMP) with respect to the origin of the lattice and for the scattering vector $\mathbf{s}=s_1\mathbf{A}^*+s_2\mathbf{B}^*+s_3\mathbf{C}^*$ are defined, respectively, by

$$F_X(\mathbf{s}) = \sum_{\text{at}(X)} f_{\text{at}}(X) e^{-2i\pi\cdot\mathbf{r}_{\text{at}(X)}\mathbf{s}} , \tag{A1a}$$

$$F_S(\mathbf{s}) = \sum_{\text{at}(S)} f_{\text{at}(S)} e^{-2i\pi\cdot\mathbf{r}_{\text{at}(S)}\mathbf{s}} , \tag{A1b}$$

$$F_M(\mathbf{s}) = \sum_{\text{at}(M)} f_{\text{at}(M)} e^{-2i\pi\cdot\mathbf{r}_{\text{at}(M)}\mathbf{s}} , \tag{A1c}$$

where f_{at} and $\mathbf{r}_{\text{at}}$ are the scattering factor and the position of an atom, respectively.

With these definitions, the structure factor of an X/S chain is given by

$$F_r(\mathbf{s}) = \left[\sum_W [F_x(\mathbf{s}) + F_s(\mathbf{s}) e^{i\pi s_3}] e^{2iW\pi s_3}\right] \times [(e^{i\pi s_3}+1)/2 + S_r(e^{i\pi s_3}-1)/2] , \tag{A2}$$

where W is the coordinate along **C**.

Assuming that the stacks of molecule do not undergo any distortion, the structure factor of a chain of molecules and of a chain of X/S is

$$\mathcal{F}_r(\mathbf{s})=F_r(\mathbf{s})+\sum_W F_M(s)(1+e^{i\pi s_3})e^{2i\pi W s_3} . \tag{A3}$$

The total scattered intensity $I(\mathbf{s})$ is given by[38]

$$I(\mathbf{s})=\sum_r \langle \mathcal{F}_{r'}(\mathbf{s})\mathcal{F}_{r+r'}(\mathbf{s})\rangle_{r'} e^{2i\pi \mathbf{s}\cdot\mathbf{r}} , \tag{A4}$$

which is usually decomposed in two terms:

$$\begin{aligned} I(\mathbf{s})&=\sum_r |\langle \mathcal{F}_r(\mathbf{s})\rangle|^2 e^{2i\pi \mathbf{s}\cdot\mathbf{r}}+\sum_r \langle [\mathcal{F}_{r'}(\mathbf{s})-\langle \mathcal{F}_r(\mathbf{s})\rangle][\mathcal{F}_{r+r'}(\mathbf{s})-\langle \mathcal{F}_r(\mathbf{s})\rangle]\rangle_{r'} e^{2i\pi \mathbf{s}\cdot\mathbf{r}} \\ &=I_{\text{Bragg}}+I_{\text{DiffScat}} . \end{aligned} \tag{A5}$$

I_{Bragg} is the value of the intensity scattered by the mean structure, which is maximum at the reciprocal points $H\mathbf{A}^*+K\mathbf{B}^*+L\mathbf{C}^*$ (H,K,L integers) and I_{DiffScat} the diffuse scattering intensity.

Using the relations

$$\langle \mathcal{F}_r(\mathbf{s})\rangle=(1+e^{i\pi s_3})\{[F_X(\mathbf{s})+F_S(\mathbf{s})e^{i\pi s_3}]/2+F_M(\mathbf{s})\}\delta(L-s_3) , \tag{A6a}$$

$$\mathcal{F}_r(\mathbf{s})-\langle \mathcal{F}_R(\mathbf{s})\rangle=(e^{i\pi s_3}-1)/2[F_X(\mathbf{s})+F_S(\mathbf{s})e^{i\pi s_3}]S_r\delta(L-s_3) , \tag{A6b}$$

and

$$\mathbf{S}_S=\sum_r S_r e^{2i\pi \mathbf{s}\cdot\mathbf{r}} , \tag{A6c}$$

one gets the intensities of the Bragg reflections and the diffuse lines:

$$\text{If } s_3=2n , \quad I_{\text{Bragg}}=|F_X(\mathbf{s})+F_S(\mathbf{s})+2F_M(\mathbf{s})|^2 , \tag{A7a}$$

$$I_{\text{DiffScat}}=0 , \tag{A7b}$$

$$\text{If } s_3=2n+1 , \quad I_{\text{Bragg}}=0 , \tag{A8a}$$

$$\begin{aligned} I_{\text{DiffScat}}&=|F_X(\mathbf{s})-F_S(\mathbf{s})|^2\sum_r \langle S_0 S_r\rangle e^{2i\pi \mathbf{s}\cdot\mathbf{r}} \\ &=|F_X(\mathbf{s})-F_S(\mathbf{s})|^2\langle S_s S_{-s}\rangle . \end{aligned} \tag{A8b}$$

APPENDIX B: GROUND STATES OF THE 2D ISING MODEL

It is known from the Mermin-Wagner theorem[39] that the ground state of a 2D system with continuous symmetry cannot be long-range ordered. For a 2D Ising system, this theorem forbids a long-ranged ordering of the spins with an incommensurate wave vector, as predicted by the mean-field analysis in the T' (Ref. 19) and P' domains of the phase diagram [Fig. 11(a)]. Therefore, in order to obtain the actual ground states of the system, we have to compare the energies of the antiferromagnetic (commensurate) spin configurations of the C and M domains (Fig. 12).

The energy per spin in the M domain is given by

$$E_M=2J_1+2J_2-2J_3-2J_4 \tag{B1}$$

and in the C domain,

$$E_C=-2J_1+2J_2-2J_3-2J_4 . \tag{B2}$$

C is the ground state if $E_C<E_M$, which yields

$$\frac{J_3}{|J_1|}+\frac{J_4}{|J_1|}>-1 \quad \text{(the equality defines the } \mathcal{S} \text{ line)} \tag{B3}$$

in the $J_1=J_2$ case.

This $\mathcal{S}$ line is shown in Fig. 11(a). It separates the stability domains of the C and M phases. As the T and P domains have to vanish at zero temperature, the disorder and Lifshitz lines are dependent on temperature and join together at the $\mathcal{S}$ line at $T=0$.

*On leave from Institute Rudjer Boskovic, Bijenicka c.54, POB 1016, 41001 Zagreb, Croatia.

[1]D. Jerome and H. J. Schulz, Adv. Phys. **31**, 299 (1982).
[2]J.-P. Pouget, *Structural instabilities in Semiconductors and Semimetals* (Academic, New York, 1988), Vol. 27.
[3]D. Jerome, A. Mazaud, M. Ribault, and K. Bachgaard, J. Phys. Lett. **41**, L95 (1980).
[4]M. Ribault, J. P. Pouget, D. Jerome, and K. Bechgaard, J. Phys. Lett. **41**, L607 (1980).
[5]K. Mortensen, Y. Tomkiewicz, T. D. Schultz, and E. M. Engler, Phys. Rev. Lett. **46**, 1234 (1981).
[6]J. B. Torrance, H. J. Pedersen, and K. Bechgaard, Phys. Rev. Lett. **49**, 881 (1982).
[7]For more recent developments see, e.g., Proceedings of the International Conference on Science and Technology of Synthetic Materials (ICSM '92), Göteborg, Sweden, August [Synth. Met. **55-57** (1992)].
[8]C. Coulon, P. Delhaes, S. Flandrois, R. Lagnier, E. Bonjour, and J. M. Fabre, J. Phys. (Paris) **43**, 1059 (1982).
[9]K. Penc and F. Mila, J. Phys. (France) IV **3**, C2-155 (1993).
[10]J. P. Pouget, in *Low-Dimensional Conductors and Superconductors,* edited by D. Jerome and L. G. Caron (Plenum, New

York, 1987).
[11]V. J. Emery, R. Bruinsma, and S. Barisic, Phys. Rev. Lett. **48**, 1039 (1982).
[12]P. Michel, A. Moradpour, P. Penven, L. Firlej, P. Bernier, B. Levy, S. Ravy, and A. Zahab, J. Am. Chem. Soc. **112**, 8285 (1990).
[13]K. V. Schubert and R. Strey, J. Chem. Phys. **95**, 8532 (1991).
[14]L. J. Martinez-Miranda, A. R. Kortan, and R. J. Birgeneau, Phys. Rev. Lett. **56**, 2264 (1986).
[15]However, increasing the size of the anion up to that of a cluster completely changes the structure and the stoïchiometry of the salts, see for example A. Penicaud, P. Batail, C. Coulon, E. Canadell, and C. Perrin, Chem. Mater. **2**, 123 (1990).
[16]D. McCullough, G. B. Kok, K. A. Lerstrup, and D. O. Cowan, J. Am. Chem. Soc. **109**, 4115 (1987).
[17]G. Saito, T. Enoki, M. Kobayashi, K. Inaeda, N. Sato, and H. Inokuchi, Mol. Cryst. Liq. Cryst. **119**, 393 (1985).
[18]P. Penven, D. Jerome, S. Ravy, P.-A. Albouy, and P. Batail, Synth. Met. **27**, B405 (1988).
[19]T. Garel, V. Ilakovac, S. Ravy, Phys. Rev. B **49**, 12 791 (1994).
[20]J. Stephenson, Can. J. Phys. **47**, 2621 (1969); J. Math. Phys. **11**, 420 (1970).
[21]J. Stephenson, Phys. Rev. B **11**, 4405 (1970).
[22]R. M. Hornreich, M. Luban, and S. Shtrickman, Phys. Rev. Lett. **35**, 1678 (1975).
[23]N. Metropolis, A. W. Rosenbluth, M. N. Rosenbluth, A. H. Teller, and E. J. Teller, Chem. Phys. **21**, 1087 (1953).
[24]B. D. Butler and T. R. Welberry, J. Appl. Crystallogr. **25**, 391 (1992).
[25]T. R. Welberry and R. Galbraith, J. Appl. Crystallogr. **6**, 87 (1973).
[26]D. Dicarlo, R.E. Thorne, E. Sweetland, M. Sutton, and J. D. Brock, Phys. Rev. B **50**, 8288 (1994).
[27]E. Canadell (private communication).
[28]P. Penven, Ph.D. thesis, Orsay, France, 1990.
[29]R. Lapouyade, J. P. Morand, D. Chasseau, C. Hauw, and P. Delhaes, J. Phys. (Paris) Colloq. **44**, C3-1235 (1993).
[30]V. Ilakovac, S. Ravy, J.-P. Pouget, W. Riess, W. Brütting, and M. Schwoerer, J. Phys. (France) IV **3**, C2-137 (1993).
[31]M. Burggraaf, H. Dragan, P. Gruner-Bauer, H. W. Helberg, W. F. Kuhs, G. Mattern, D. Mueller, W. Wendl, A. Wolter, and E. Dormann, Z. Phys. B **96**, 439 (1995).
[32]K. F. Thier and M. Mehring, Phys. Rev. B **50**, 2142 (1994).
[33]W. Brütting, W. Riess, and M. Schwoerer, Ann. Phys. **1**, 409 (1992).
[34]V. Ilakovac, S. Ravy, J.-P. Pouget, C. Lenoir, K. Boubekeur, P. Batail, S. Dolanski Babic, N. Biskup, B. Korin-Hamzic, S. Tomic, and C. Bourbonnais, Phys. Rev. B **50**, 7136 (1994).
[35]R. Moret, E. Tronc, M. Huber, and R. Comes, Philos. Mag. B **38**, 105 (1978).
[36]R. De Ridder, G. Van Tendeloo, D. Van Dick, and S. Amelynckx, J. Phys. (Paris) Colloq. **38**, C7-178 (1977).
[37]T.R. Welberry and R. L. Withers, J. Appl. Crystallogr. **20**, 280 (1987).
[38]A. Guinier, *X-ray Diffraction in Crystals, Imperfect Crystals and Amorphous Bodies* (Freeman, San Francisco, 1963) or (Dover, New York, 1994), for a recent reedition.
[39]N. D. Mermin and H. Wagner, Phys. Rev. Lett. **17**, 1133 (1966).

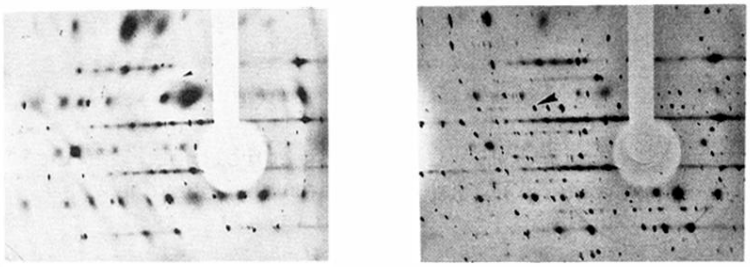

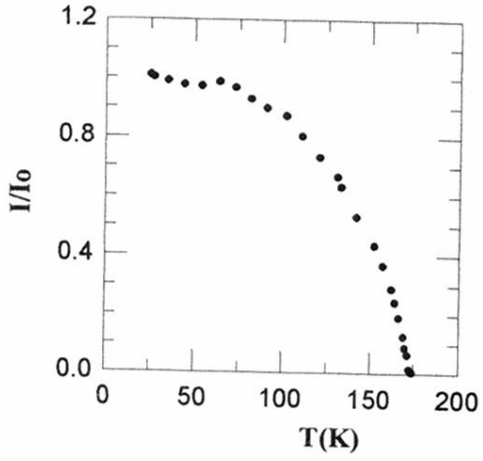

FIG. 10. Fixed-film fixed-crystal pattern of $(TMP)_2AsF_6$-CH_2Cl_2 single crystal at room temperature (a) and at 11 K (b). A small arrow points towards $2k_F$ diffuse scattering line and a large one to a low-temperature satellite reflection. Temperature variation of the normalized intensity of a satellite with temperature (c).

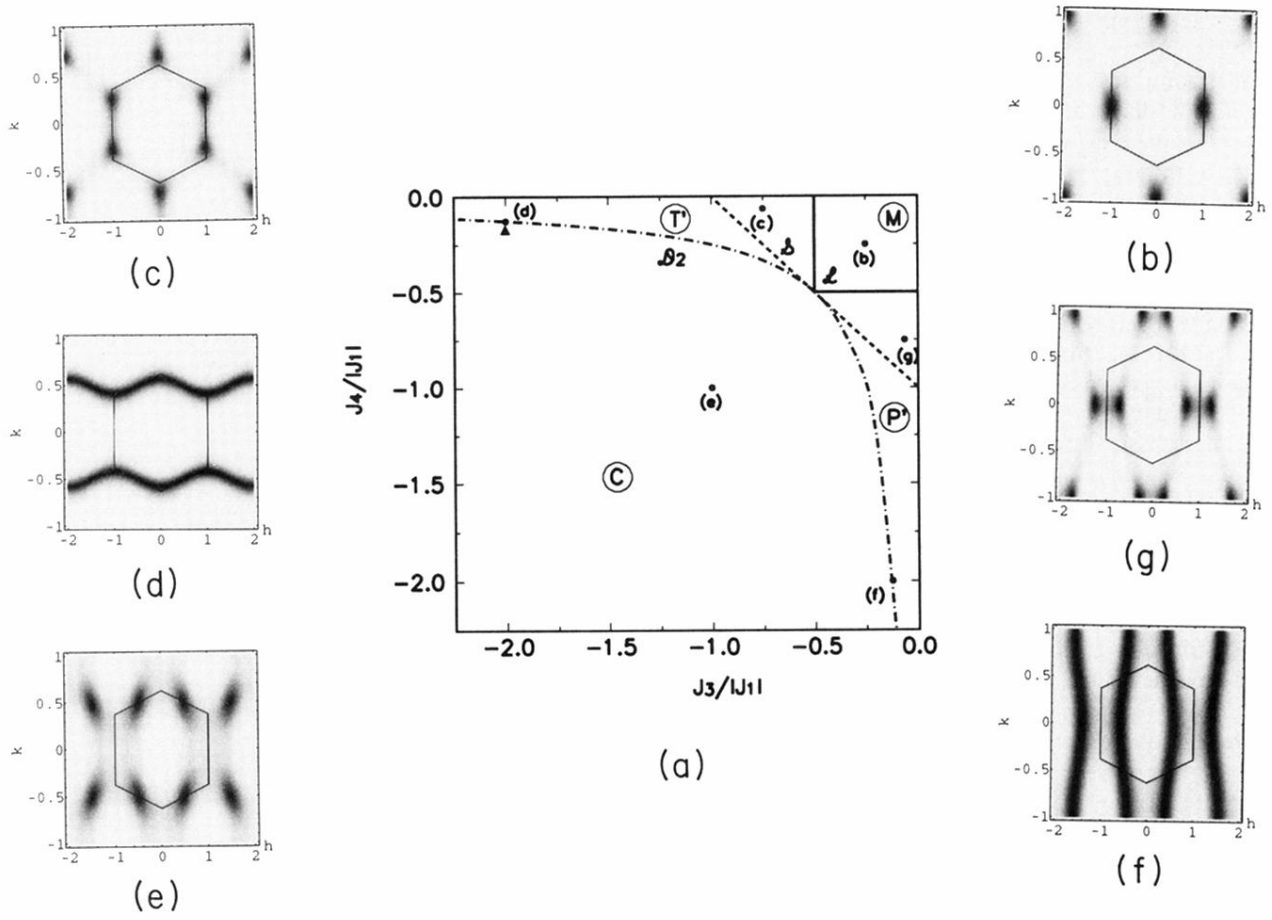

FIG. 11. (a) Mean-field $(J_3/|J_1|, J_4/|J_1|)$ phase diagram. The full lines ($\mathcal{L}$) are the Lifshitz lines, the dashed-dotted line ($\mathcal{D}_2$) is the disorder line of the second kind and the dashed ($\mathcal{S}$) line separates and M and C ground-state stability domains. The circled letters indicate the locus of the scattered intensity maxima in the 1st BZ of Fig. 6(b). The triangle indicates the position of the $(TMP)_2PF_6$-CH_2Cl_2 system in this (temperature-independent) diagram. (b), (c), (d), (e), (f), (g): Typical scattered intensity calculated at the points indicated in (a). A scheme of the 1st BZ is indicated on each figure.

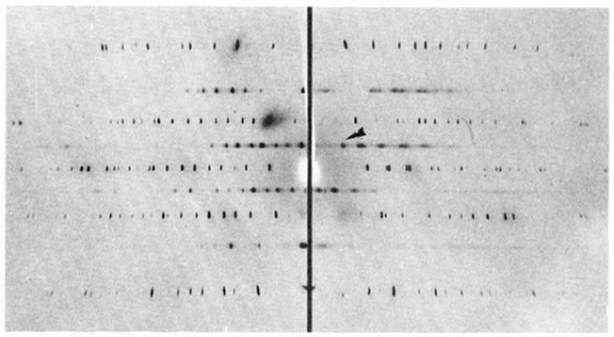

(a)

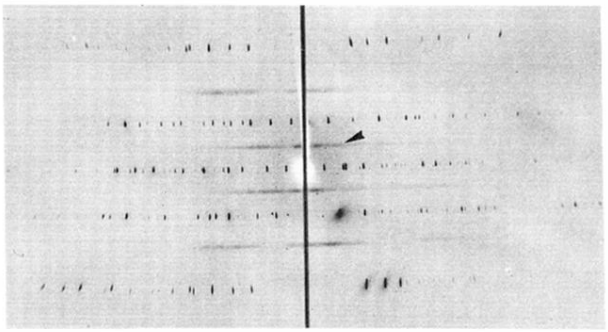

(b)

FIG. 3. Room-temperature oscillating ($\Delta\omega = 40°$) crystal photographs of $(CPP)_2PF_6$-CH_2Cl_2 (a) and $(TMP)_2PF_6$-CH_2Cl_2 (b). The c axis is vertical. The arrows point towards the $l = 1/2$ diffuse lines.

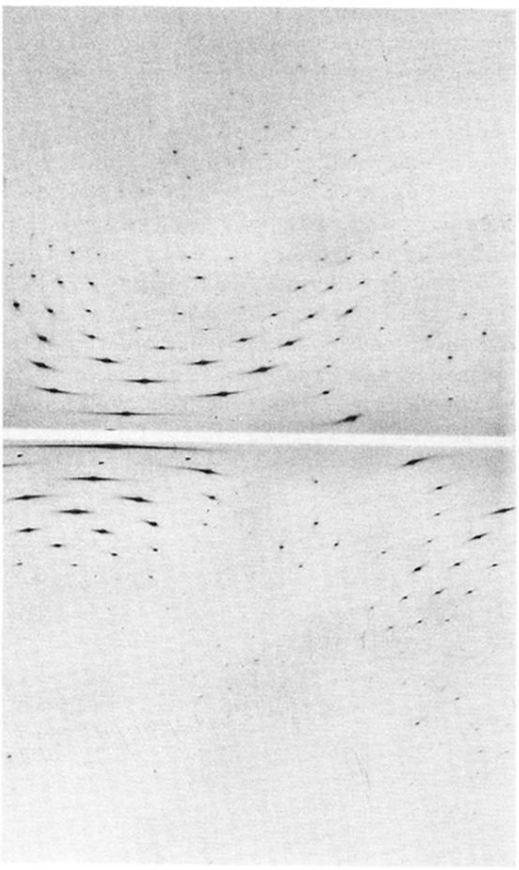

FIG. 4. (a) Weissenberg diffraction pattern of the $l=0.5$ layer of $(CPP)_2PF_6$-CH_2Cl_2. (b) Scattering intensity profile of the (3,0,0.5) reflection in the $\mathbf{b}^*$ direction. The full line represents a fit by a square root of a Lorentzian function, while dotted and dashed lines represent Lorentzian functions.

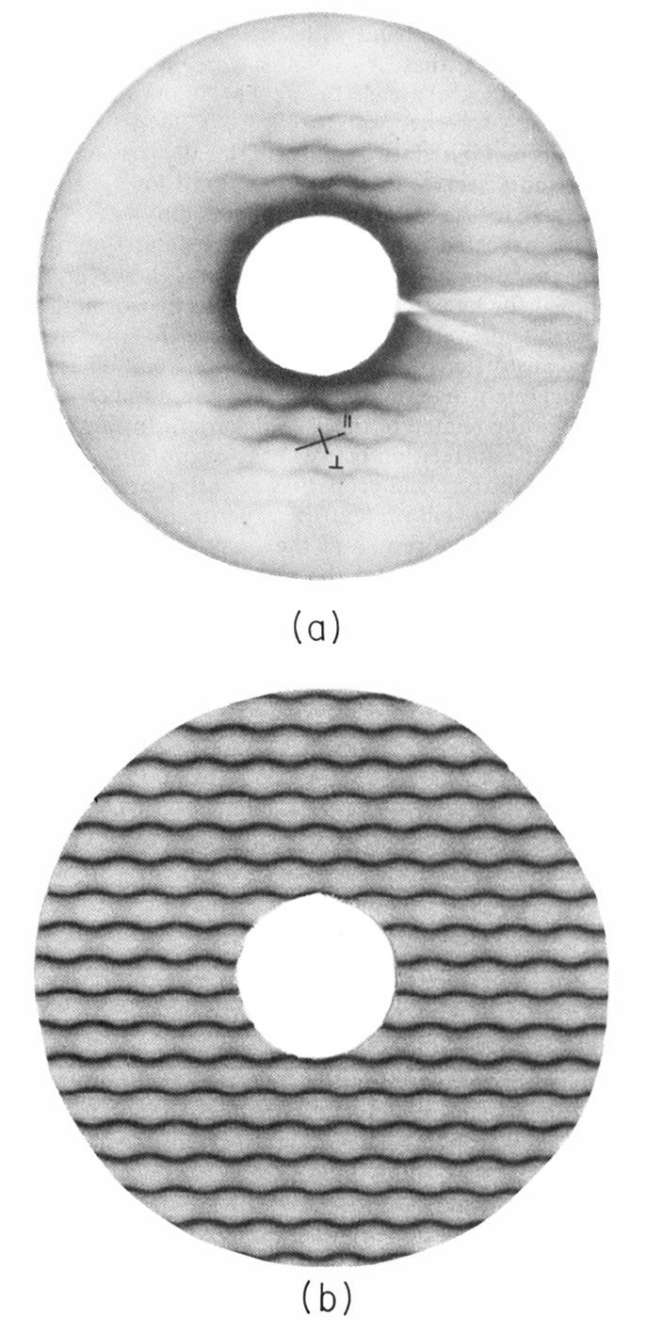

FIG. 5. Precession pattern of $(TMP)_2PF_6$-CH_2Cl_2 (a) and its best simulation (b). $\perp$ and $\parallel$ represent the directions of scans described in the text.

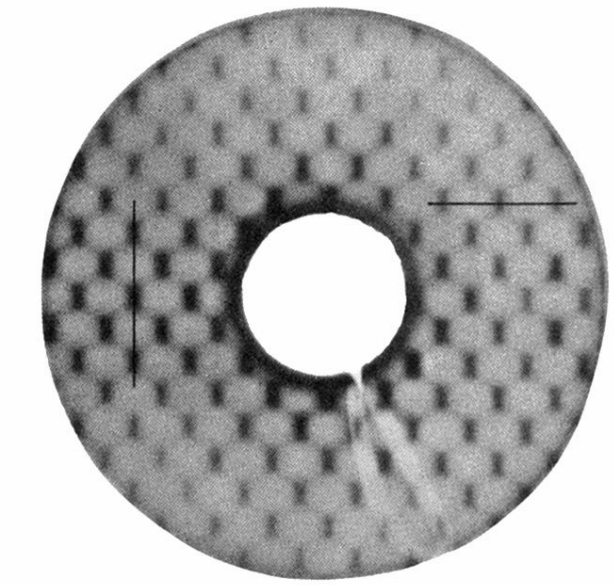

(a)

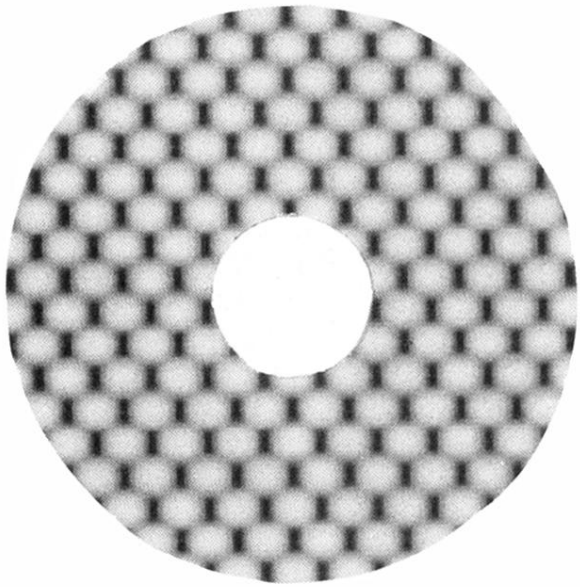

(b)

FIG. 7. Precession pattern of $(TMP)_2AsF_6^- CH_2Cl_2$ (a) and its best simulation (b). Vertical and horizontal lines represent the directions of the microdensitometer scans showed in Fig. 8.